





Feedback-induced locking in semiconductor lasers with strong amplitude-phase couplingJan Hausen ^{1,*}, Bastian Herzog ², Alexander Nelde ², Stefan Meinecke ¹, Nina Owschimikow,² and Kathy Lüdge ^{1,†}¹*Institute of Theoretical Physics, Technische Universität Berlin, Hardenbergstraße 36, 10623 Berlin, Germany*²*Institute of Optics and Atomic Physics, Technische Universität Berlin, Hardenbergstraße 36, 10623 Berlin, Germany*

(Received 6 January 2021; accepted 18 March 2021; published 16 April 2021)

The influence of optical feedback on semiconductor lasers has been a widely studied field of research due to fundamental interests as well as the optimization of optical data transmission and computing. Recent publications have shown that it is possible to induce a periodic pulselike output in quantum-dot and quantum-well laser diodes based on the locking of the external cavity modes and the relaxation oscillation frequency. We present an in-depth analysis of this effect. We choose submonolayer quantum dots as a gain system, as these provide a relatively strong amplitude-phase coupling, which has proven to be very beneficial for these locking effects to occur. By introducing an alternative theoretical model, we can correctly reproduce the essential features of the gain system and validate them by comparison to our experimental results. From this starting point we can further explore how the staircase behavior of the oscillation frequency with increasing pump current can be influenced by changing various laser parameters. The staircase behavior is induced by a reordering of the Hopf bifurcations giving birth to the regular pulselike oscillations.

DOI: [10.1103/PhysRevA.103.043511](https://doi.org/10.1103/PhysRevA.103.043511)**I. INTRODUCTION**

Semiconductor lasers have become a central component of today's optical data transfer due to their well-established production and high transmission rates [1,2]. A scheme to severely influence the dynamics of these lasers is direct optical feedback [3]. This method, on the one hand, can be used to stabilize the laser output [4–6] and reduce the linewidth of the laser [7–9] or the timing jitter of a pulsed output [10–13]. On the other hand, it is a well-established approach to drive the laser into chaotic regimes [14–18], which can be applied, e.g., for the encoding of data [19,20] or has to be accounted for as a detrimental effect in communication lines. Moreover, lasers subject to feedback are also an interesting candidate to implement computation schemes such as reservoir computing [21–24].

Recent works on quantum-dot and quantum-well lasers under optical feedback have shown that a locking between the external cavity modes and the relaxation oscillation frequency of the continuous-wave (cw) solution can lead to a periodic pulselike laser output [25,26]. Similar effects have also been observed for laser diodes with a three-dimensional (3D) gain medium [27–32] as well as quantum-dash lasers under optoelectronic feedback [33,34]. As the deterministic generation mechanism of the periodic states lies within the locking of the internal and external frequency components and therefore requires them to be close together, these oscillations are different from the high-frequency oscillations occurring for short optical feedback [35], pure frequency oscillations [31,36], or noise-driven low-frequency oscillations [37,38]. Moreover, the analysis of the locking effect suggested that a high damping and a strong amplitude-phase coupling are

very beneficial for the transition from cw lasing to periodic dynamics at experimentally observable feedback strengths [26,39]. However, the resulting oscillations mostly occur as an unwanted effect for applications, as the resulting pulselike oscillations are not of the quality of high-performance mode-locked devices [40–42] or optical solitons [43,44] or rogue waves [45].

In order to underline the generality of this feedback effect in terms of the choice of the gain medium, we utilize a laser diode based on submonolayer quantum dots (SMLQDs) [46,47]. These 0D localization centers have higher areal density than conventional quantum dots [1,48,49] and therefore provide a higher gain per unit length [50]. Furthermore, these structures exhibit a strong amplitude-phase coupling, i.e., high α -factor, and preserve advantages such as suppressed carrier diffusion, high gain and phase recovery, and low degradation rates [51–56]. Submonolayer quantum dots have been successfully implemented as a gain medium in laser diodes as well as external cavity lasers [57–60].

In this paper we theoretically and experimentally investigate a SMLQD laser diode subject to filtered optical feedback at intermediate feedback lengths with respect to the relaxation oscillation timescale ($\tau = 3.8$ ns). We observe delay-induced higher-order locking effects also found for quantum-well and quantum-dot gain media [25,26]. This highlights that the applied optical feedback is the driving force of the locking as it has a much greater influence than the choice of the gain medium. We support the experimental evidence by developing a relatively simple theoretical SML-QD model which retains the most relevant timescales for the locking effects, i.e., the relaxation oscillations [52], and validate it by comparison to experimental findings. From that starting point, we gain physical insight into the emergence of the feedback-induced pulselike oscillations by a detailed bifurcation analysis. Hence, we are able to unravel the underlying generation mechanism of a staircase dependence of the

*hausen@campus.tu-berlin.de

†kathy.luedge@tu-berlin.de

oscillation period on the pump current. Additionally, we discuss how the relaxation oscillations can be altered to influence the staircase and furthermore discuss the role of the amplitude-phase coupling for the occurrence of the pulslike states in a large parameter regime. The staircase behavior can potentially be exploited to construct a tunable photonic microwave source, which only relies on a single laser device [34,61,62]. Furthermore, the generality and deeper understanding of the locking effect with respect to several parameters can be of use in applications which require a stable continuous-wave output and optical feedback occurs as a detrimental effect.

II. EXPERIMENTAL SETUP AND LASER DEVICE

As their name suggests, submonolayer quantum dots are grown by repeatedly depositing layers of a lower-band-gap material in between a higher-band-gap material (e.g., InAs layers on GaAs bulk) [46,47]. These layers have a thickness below one monolayer (ML). Due to a vertically correlated growth caused by local strain effects, 0D localization centers form with a high areal density providing a high gain per unit length [51–53]. The investigated SMLQD *p-i-n* laser diode was grown utilizing metal organic vapor phase epitaxy. The active section consisted of 15-fold deposition of 0.73 ML InAs and 1.13 ML GaAs, respectively. This results in an active section width of 8 nm, embedded in 10-nm spacers of GaAs bulk material. A shallow etched waveguide provided single-mode operation via gain guiding. The laser diode had a longitudinal cavity length of 0.5 mm. The optical power spectra were measured with a fiber-coupled optical spectrum analyzer (Hewlett Packard 70952B) and the radio-frequency (rf) spectra were obtained using a fiber-coupled high-speed photodetector with a bandwidth of $\Delta f_{\text{PD}} = 12$ GHz (New Focus 1544-A-50) read out by an electrical spectrum analyzer (Rohde & Schwarz FSC3 Spectrum Analyzer) of which the resolution bandwidth was set to $\Delta f_{\text{RBW}} = 1$ MHz and video bandwidth to $\Delta f_{\text{RBW}} = 1$ kHz for all measurements. Time traces of the laser dynamics were recorded utilizing a real-time oscilloscope with a bandwidth of $\Delta f_{\text{osc}} = 1$ GHz. The Fabry-Pérot laser was installed in the external cavity setup schematically shown in Fig. 1(a). By adding an etalon with a transmission linewidth of 0.4 nm at full width at half maximum into the feedback arm (left), it was possible to select a single lasing mode for the feedback. The optical spectral properties of the free-running device are displayed in Figs. 1(b) and 1(c). A highly resolved spectrum is shown in Fig. 1(b), with a blue line indicating the mode for which the maximum feedback was possible. The low-resolution spectra for different pump currents in Fig. 1(c) clearly indicate the emergence of lasing modes of the free-running device above the threshold of $J_{\text{th}} = 6.4$ mA.

III. THEORETICAL MODEL

In order to reproduce the dynamics of the investigated device we develop a model based upon the phenomenological approach carried out in [52,55], where the SMLQDs were divided into subgroups based on their confinement energy and their respective density of states. To arrive at the model

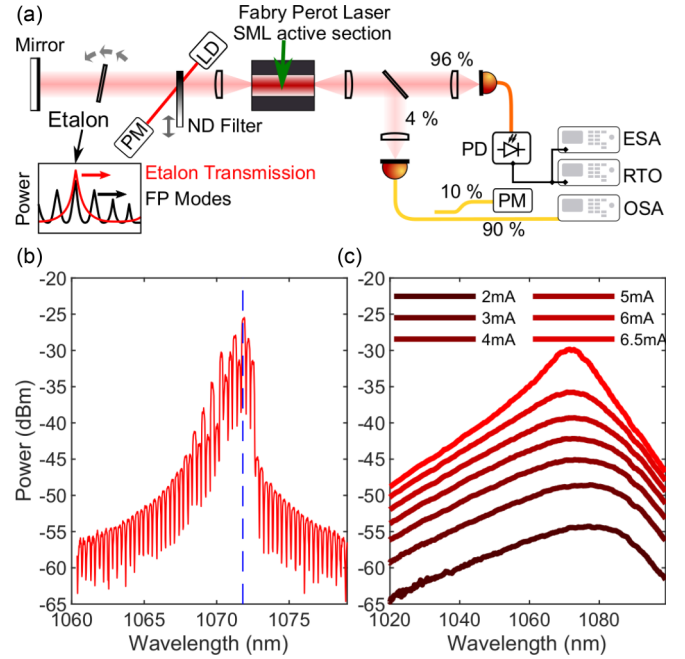


FIG. 1. (a) Experimental setup utilized to investigate the effect of feedback on a SMLQD laser. An etalon in the feedback arm (left) enables single-mode operation. The detection arm (right) includes an electrical spectrum analyzer (ESA), an optical spectrum analyzer (OSA), and a real-time oscilloscope (RTO). The attenuation of the neutral density (ND) filter is determined using a photodetector (PM) and a laser diode (LD). (b) Optical spectrum (resolution 0.08 nm) of the free-running laser, with the investigated mode to which the etalon was tuned marked by a vertical blue line. (c) Coarsely resolved spectrum (resolution 2 nm) at different pump currents, indicating the emergence of a lasing mode closely above the threshold of $J_{\text{th}} = 6.4$ mA.

presented here, an average over the submonolayer subgroups is performed, which is justified by the fact that the investigated locking effects occur on a much longer timescale than the diffusive coupling between the subgroups [52]. The averaging also leads to the neglect of spectral hole burning, which can be justified by the fact that in the investigated regimes of low pump currents $J < 1.5J_{\text{th}}$, the gain increases linearly with J and no gain saturation is observed [51,56]. The amplitude-phase coupling, including the role of the inactive states, is approximated by a constant large α -factor. This also results from the lateral coupling and the size of the inactive reservoir leading to a higher phase response compared to conventional quantum-dots [50,55]. Another critical aspect to take into account is the differing relaxation rates of bulk and SMLQD states in the gain. The model describes the dynamics of the device in terms of the complex intracavity, dimensionless electric field $E(t)$ within the slowly varying envelope approximation, the submonolayer quantum-dot occupation probability $\rho(t)$, and the bulk reservoir charge-carrier density $n(t)$. The resulting equations read

$$\begin{aligned} \frac{d}{dt}E(t) = & \frac{1}{2} \{g[2\rho(t) - 1](1 - i\alpha) - T_{\text{ph}}^{-1}\}E(t) \\ & + \frac{K}{2T_{\text{ph}}} e^{iC} E(t - \tau) + F(t), \end{aligned} \quad (1)$$

TABLE I. Parameter values used for the theoretical investigation of the SMLQD device, unless indicated otherwise.

Symbol	Value	Symbol	Value
J_{th}	$379 \times 10^{11} \text{ ns}^{-1} \text{ cm}^{-2}$	J_{tr}	$223 \times 10^{11} \text{ ns}^{-1} \text{ cm}^{-2}$
$\bar{\epsilon}_{SML}$	0.06 eV	h_{bulk}	53.0 nm
α	5	T	300 K
n_{SML}	$3.3 \times 10^{11} \text{ cm}^{-2}$	m^*	$0.07m_e$
τ	3.8 ns	g	185 ns^{-1}
T_{ph}	9 ps	T_ρ	0.066 ns
T_n	0.5 ns	R_0	240 ns^{-1}
K	0	C	0

$$\frac{d}{dt}\rho(t) = -\frac{1}{T_\rho}\rho(t) + R[\rho_{eq}(t, n) - \rho(t)] - g[2\rho(t) - 1]|E(t)|^2, \quad (2)$$

$$\frac{d}{dt}n(t) = -\frac{1}{T_n}n(t) + \frac{J}{h_{bulk}} - \frac{2n_{SML}}{h_{bulk}}R[\rho_{eq}(t, n) - \rho(t)] \quad (3)$$

where g is the differential gain coefficient, α the amplitude-phase coupling coefficient, T_{ph} the photon lifetime, K the relative feedback strength, C the relative feedback phase, τ the external cavity round-trip time (feedback time), $F(t)$ a δ -correlated complex Gaussian Langevin noise term, T_ρ the SMLQD lifetime, h_{bulk} the effective bulk reservoir thickness, R the SMLQD-bulk coupling rate, J the pump current density, T_n the bulk carrier lifetime, n_{SML} the SMLQD area density, and $\rho_{eq}(t, n)$ the SMLQD quasiequilibrium occupation probability, which follows a Fermi function of which the chemical potential depends on the charge carrier density n . Details on the determination of the SMLQD equilibrium occupation probability $\rho_{eq}(t, n)$ are given in Appendix A. The SMLQD-bulk coupling rate is modeled with a quadratic dependence on the pump current density

$$R = R_0 \left(\frac{J}{J_{tr}} \right)^2, \quad (4)$$

where J_{tr} is the transparency pump current and R_0 is the coupling rate at transparency. The quadratic dependence of R on the pump current J models the behavior of the charge-carrier scattering rates from the 3D bulk reservoir into the 0D SMLQD states [52,63]. The feedback term is included as proposed by Lang and Kobayashi [64–69] and is valid for the low feedback strength ($K < 0.1$) investigated in this paper. It has to be pointed out that the laser is modeled to be in single-mode operation and therefore the feedback is also single mode. This is supported by the fact that by tuning the etalon to a desired mode as indicated in Fig. 1(b), already low feedback is sufficient to suppress the other modes (see Appendix C).

In order to adjust the parameters relating the SMLQD model (1)–(3) and the experimentally investigated device, we measure the relative intensity noise (RIN) spectrum at different pump currents without feedback (multimode operation) as shown in Fig. 2(a). Applying the fit proposed in [70] and indicated by black lines in Fig. 2(a), we are able to extract the relaxation oscillation (RO) frequency of the free-running laser

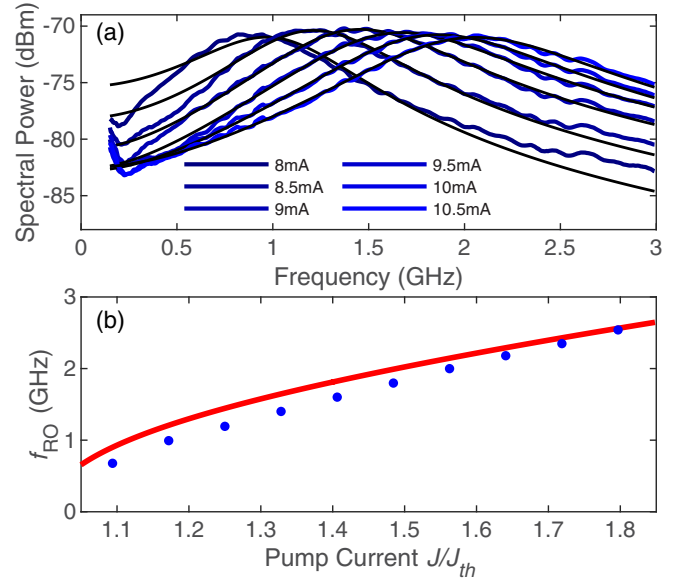


FIG. 2. (a) Relative intensity noise spectra of the free-running laser measured at different pump currents given in the legend, with a noise-equivalent power of $27 \text{ pW}/\sqrt{\text{Hz}}$. The RIN spectra were fitted according to the routine introduced in [70,71] to extract the relaxation oscillation frequency at each pump current. (b) Blue circles show the experimentally determined relaxation oscillations and the red line shows the evolution of the relaxation oscillation frequency with increasing pump current J (normalized to the lasing threshold J_{th}) obtained by implementing the model (1)–(3) in DDE-BIFTOOL. The parameters used are shown in Table I.

from each RIN spectrum. The resulting experimentally determined relationship of the RO frequency and the pump current is shown by the blue circles in Fig. 2(b). Implementing the system (1)–(3) in the path continuation software DDE-BIFTOOL [72] makes it possible to continue the cw solution in J . We execute this in the regime of zero feedback $K = 0$ and identify the RO frequency at each pump current as the imaginary part of the largest nontrivial (nonzero) eigenvalue. The eigenvalues can be found by applying a linear stability analysis for each point of the cw solution branch. In order to adapt the parameters used in the theoretical model to the investigated device we adjust the parameters so that the simulated relaxation oscillations fit well to the experimentally obtained values. On that account, we slightly adjust the relaxation times and the coupling R_0 obtained for a similar laser device presented in Ref. [52]. The parameters chosen in the further course of this paper are given in Table I, if not indicated otherwise. We achieve good qualitative agreement between the relaxation oscillation frequencies determined via experimental (blue circles) and theoretical methods (red line) as displayed in Fig. 2(b). We choose a high α -factor to take into account the contribution of the inactive SMLQDs, which is also justified by experimental findings predicting an α -factor between 2.5 and 8 for SMLQDs [55].

IV. EMERGENCE OF PERIODIC OSCILLATIONS

When introducing single-mode feedback to the SMLQD laser device we find that above a critical feedback strength

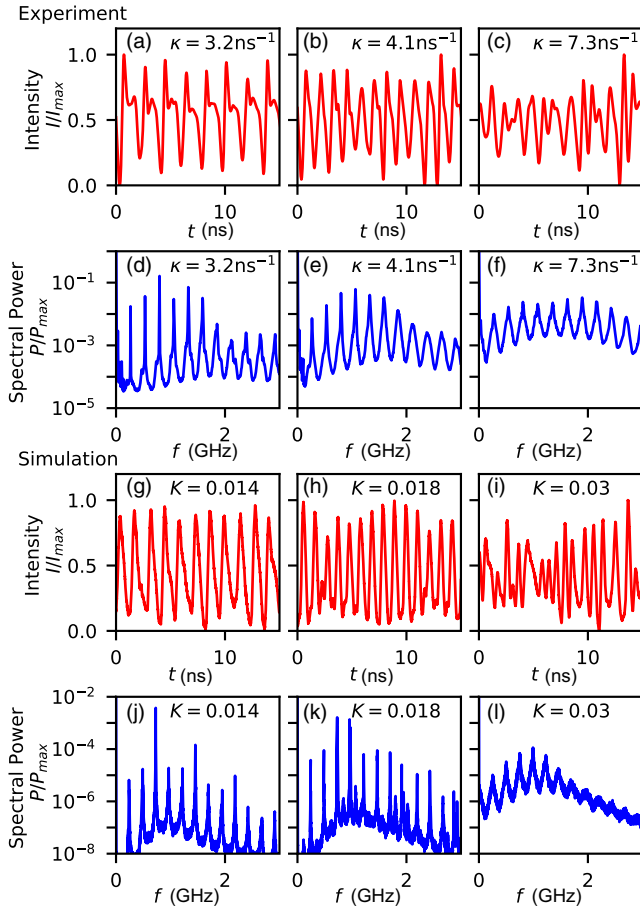


FIG. 3. (a)–(f) Experimentally measured time series and corresponding normalized rf spectra at a pump current of $J/J_{\text{th}} = 1.4, 1.4, 1.25$ from left to right. (g)–(l) Simulated data that qualitatively reproduce the experimentally obtained time series and spectra, with pump currents of $J/J_{\text{th}} = 1.09, 1.11, 1.11$ from left to right. All other parameters are as given in Table I. The minimum intensity has been subtracted as an offset.

the cw dynamics switches to a periodic orbit characterized by a pulslike laser output, as shown in real-time oscilloscope traces of the laser intensity $I = |E|^2$ in Figs. 3(a) and 3(b). The measurements were taken at increasing feedback rates of $\kappa = 3.2$ and 4.1 ns^{-1} , where κ is the effective feedback rate calculated from the differences in the laser P - I curve of the laser device under feedback and in freerunning operation (see Appendix B). It is possible to identify a transition from a pulslike regular periodic orbit to a more irregular or chaotic behavior at increasing feedback strength. This is also supported by the corresponding rf spectra shown in Figs. 3(d)–3(f). At low frequencies ($f < 1.5 \text{ GHz}$) we clearly obtain mode peaks several magnitudes above the background. These modes are separated by approximately $1/\tau = 0.26 \text{ GHz}$, i.e., the inverse of the feedback time ($\tau = 3.8 \text{ ns}$). At higher feedback strengths the peak power of the modes decreases drastically relative to the background [see Fig. 3(e)]. This evolution continues when increasing the feedback strength even further, as shown in the rf spectrum in Fig. 3(f) obtained at $\kappa = 7.3 \text{ ns}^{-1}$, which corresponds to the chaotic time series

in Fig. 3(c). The transition of the dynamics with increasing feedback strength can qualitatively be reproduced utilizing the introduced SMLQD laser model. At low feedback strength we find regular pulslike solutions, which are characterized by strong locking peaks at the dominant frequencies in the rf spectrum as indicated in Figs. 3(g) and 3(j). With increasing feedback strength the locking is less pronounced [see Fig. 3(l)] and we therefore find chaotic solutions as shown by the time series in Fig. 3(i).

This phase-locking effect, in which the phases of external cavity modes (ECMs) and the relaxation oscillation lock, was analogously found when investigating quantum-dot and quantum-well lasers [25,26] as well as optoelectronic feedback [33,34]. Our findings also support the claim that a high damping, also typical for SMLQD lasers [52], is beneficial for this locking effect to occur at intermediate feedback strengths without generating chaotic dynamics [26,73]. Furthermore, experimental and theoretical findings as well as this work suggest an intermediate feedback length of $1 \text{ ns} < \tau < 10 \text{ ns}$ close to the relaxation oscillation period being advantageous for this type of locking effects [25,26,30,32,74]. For a more in-depth analysis of the underlying dynamical transitions we continuously decrease the feedback rate starting from the maximum achievable value and measure the rf spectra of the laser output at each feedback strength. The result of the experimentally obtained data for different pump currents is indicated in the 2D plots in Figs. 4(a)–4(c), with the color code indicating the spectral power. One can note narrow locking peaks several magnitudes above the background in an intermediate region of feedback strengths between $\kappa = 1.5$ and 4 ns^{-1} , which indicates the presence of regular periodic orbits in this regime. At higher feedback strengths, the background increases and the peaks broaden, suggesting chaotic dynamics. With increasing pump currents from Fig. 4(a) to Fig. 4(c), the onset of the chaotic dynamics shifts to higher feedback strengths. Applying the theoretical model, we can also predict this feedback effect, as the calculated spectra show the same behavior [Figs. 4(d)–4(f)]. At low feedback ($0.01 < K < 0.05$) sharp and well-separated peaks of the oscillatory modes can be found. However, when increasing the feedback strengths, the modes smear out and chaotic behavior emerges, with the boundary between periodic orbits and chaotic dynamics slightly shifting to higher K with increasing pump current.

By performing further sweeps of the feedback rate while measuring the rf spectra for different pump currents we can also get a broader overview of the dynamics in the 2D (J, κ) plane. We distinguish the different dynamical regimes according to their rf spectra and cross-check with the measured time series of the laser output. The result is presented in Fig. 5. We find that for all pump currents the device turns from cw dynamics to a periodic output state. As described before, the laser destabilizes into a chaotic state at higher feedback rates (gray areas in Fig. 5). The transition to chaos, either mediated by a period-doubling cascade or quasiperiodic transition, is a well-known feedback effect [32,73,75], whereas the locking behavior at intermediate feedback strengths is the same effect found for quantum-dot, quantum-well, or 3D bulk laser diodes under optical feedback [25–27,29,31,34,39].

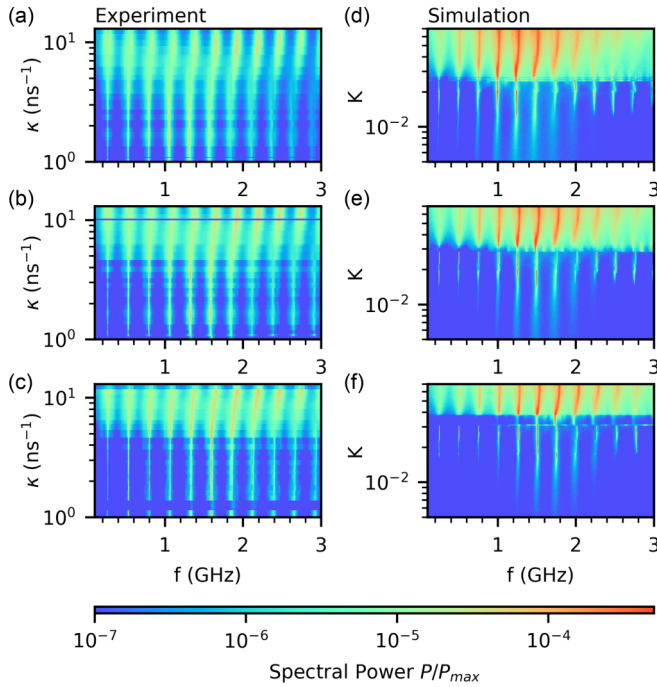


FIG. 4. (a)–(c) Experimentally obtained rf spectra at different feedback rates κ (see Appendix B). The normalized spectral power is given by the color code. The pump current was increased from top to bottom according to $J/J_{th} = 1.33, 1.41, 1.48$. (d)–(f) The rf spectra generated by direct numerical integration of the SMLQD model at different feedback strengths K , with increasing pump currents from top to bottom $J/J_{th} = 1.19, 1.26, 1.32$. The spectral power of the experimental data was multiplied by 10^3 for better comparability. All other parameters are as given in Table I.

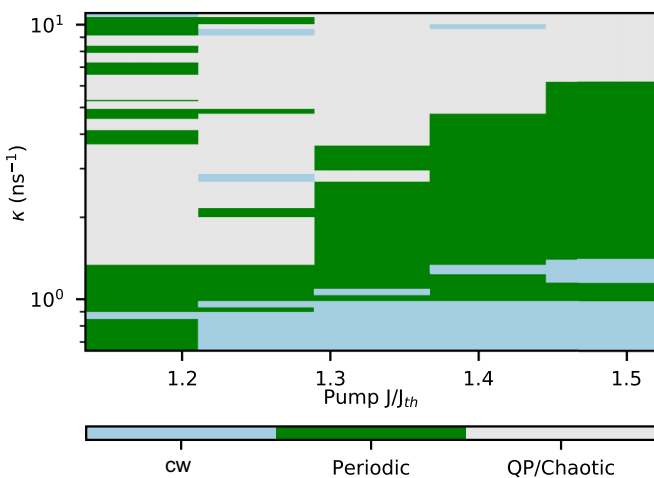


FIG. 5. Experimentally obtained map of the laser dynamics in the (J, κ) plane. The dynamical regimes are distinguished according to the rf spectra: Continuous-wave dynamics (cw) is characterized by a low-rf signal, periodic dynamics is characterized clear locking peaks with a low background [Fig. 3(d)], and chaotic or quasiperiodic (QP) dynamics refers to broadened spectral peaks and a high background [Fig. 3(f)].

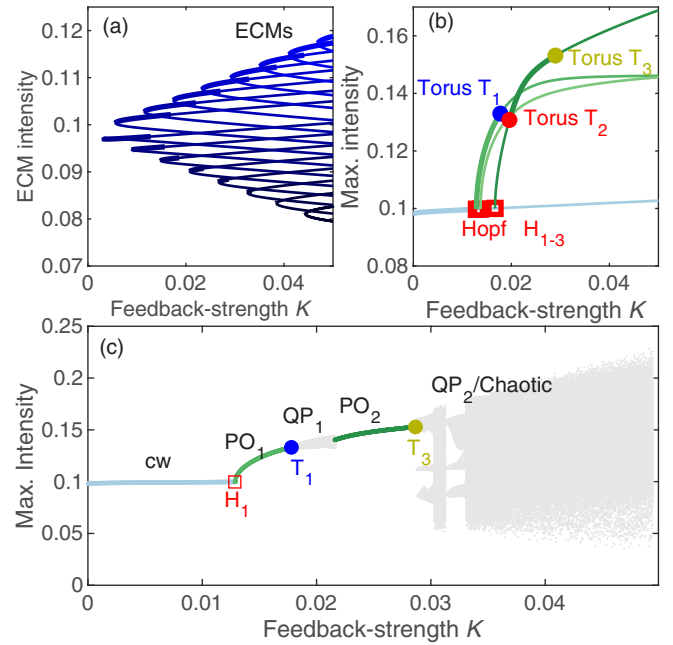


FIG. 6. One-dimensional bifurcation diagram showing the maximum intensity as a function of the feedback strength K for (a) the continuous-wave ECM solutions and (b) the cw solution (cyan) and periodic orbits (green). Thick (thin) lines denote stable (unstable) dynamics. The three periodic orbits in (b) are born in subsequent Hopf bifurcations H_{1-3} along the cw branch and can be distinguished according to the oscillation period of the born solutions, separated by integer multiples of the inverse feedback time $n/\tau = 0.26$ GHz. The torus bifurcations T_{1-3} are marked by the colored circles. (c) Dynamics obtained performing a direct numerical integration (upsweep), showing the unique intensity maxima found in 200 external cavity round-trips at each K . Chaotic or quasiperiodic regimes are indicated in gray. All parameters are as in Table I and $J/J_{th} = 1.19$.

V. BIFURCATION ANALYSIS

In order to understand the generation mechanisms of the different dynamical regimes, we investigate the role of the gain g , the pump current J , and the α -factor by performing direct numerical integrations as well as path continuation utilizing DDE-BIFTOOL [72]. We find that at the low feedback strengths investigated already a high number of ECMs are stable, as indicated by the 1D bifurcation diagrams displaying the intensity of the ECMs as a function of the feedback strength in Fig. 6(a). This behavior is expected from various analyses of the Lang-Kobayashi-type feedback implementation [64,66,76]. The stability of several ECMs at these feedback strengths suggests a high influence of the feedback on the laser dynamics. Hence, when continuing the cw solution of the solitary laser, we find that after several ECMs have become stable ($K > 0.015$) subsequent Hopf bifurcations appear, leading to a pulselike laser output [see green branches in Fig. 6(b)]. Compared to the case of standard laser diodes [30,39,74], the Hopf bifurcations appear very close after one another on the cw branch and the stable periodic orbits are not connected to the ECMs or born from bifurcations along them. Therefore, this behavior is similar to the case of optoelectronic feedback [34]. However, periodic orbits born from the Hopf

bifurcations along the ECMs also exist. These turn unstable very close to the bifurcation point in the investigated parameter regime.

The frequency of the periodic orbits born in the Hopf bifurcations along the cw branch is separated by the inverse of the feedback time $1/\tau = 0.26$ GHz. However, these bifurcations do not necessarily appear ordered with respect to the frequency as an increase in pump current leads to a reordering of the Hopf bifurcations along the cw branch, which is discussed in the subsequent section. We also investigate the direct numerical integration of the system sweeping up the feedback strength, i.e., increasing the feedback strength in small steps and using the dynamics of the previous step as the initial condition of the next to emulate the experiment. The result is shown in Fig. 6(c). In between the periodic orbits with different frequency, a quasiperiodic or chaotic regime is stable, resulting from the T_1 torus bifurcation of the first periodic orbit. However, this regime destabilizes at slightly higher feedback strength ($K \approx 0.022$) and the system stabilizes on the second regular periodic orbit, as expected from the path continuation in Fig. 6(b). As for laser diodes with 3D gain material, a route to chaos can be seen at higher feedback strength [27,75].

In order to reproduce the experimental results shown in Fig. 5 and get deeper insight into the dynamics, we also perform numerical scans of the dynamics in the (J, K) plane. The results are presented in Fig. 7, where different dynamics can be distinguished according to the color code as before. Generally, we can reproduce the experimentally observed influence of the feedback. At the investigated pump currents, the laser first transitions from the cw state to a periodic regime and then turns to a chaotic output at higher feedback strengths. Moreover, we find that the general bifurcation scenario related to a variation in feedback strength is not drastically changed when altering the pump current. The pump current for which the 1D bifurcation diagram is shown in Fig. 6(b) is indicated by the vertical black dotted line in Fig. 7(a). However, the first periodic orbit [green areas in Fig. 7(a)] stabilizing from the cw solution (light blue) changes as the Hopf bifurcations along the cw branch swap their positions [H_1 , red lines in Fig. 7(a)], when the pump current is altered. Hence, periodic orbits (POs) with different frequencies stabilize at different pump values, which is indicated by the varied shading of the periodic orbit regimes (green). As mentioned before, the frequencies of the POs differ by integer multiples of the inverse feedback time. We note that the periodic orbits stabilizing first at lower pump currents stabilize second at slightly higher pump currents, as indicated by the outstretched green areas at higher feedback strengths. The shift of the transition point between cw lasing and pulsed or chaotic behavior to higher feedback strengths with increasing pump current was also found for other Lang-Kobayashi-type feedback systems [73].

The torus bifurcations which destabilize the first periodic regime when increasing the feedback strength K [see torus T_1 in Fig. 6(b)] are indicated as dashed lines in Fig. 7(b). They are born at the intersection points of two Hopf lines [see blue circles in Fig. 7(a)]. One of the intersecting Hopf bifurcations is giving birth to the periodic orbit destabilized by the T_1 torus bifurcation. The other Hopf line is related to the Hopf bifurcation point existing closest to the lasing

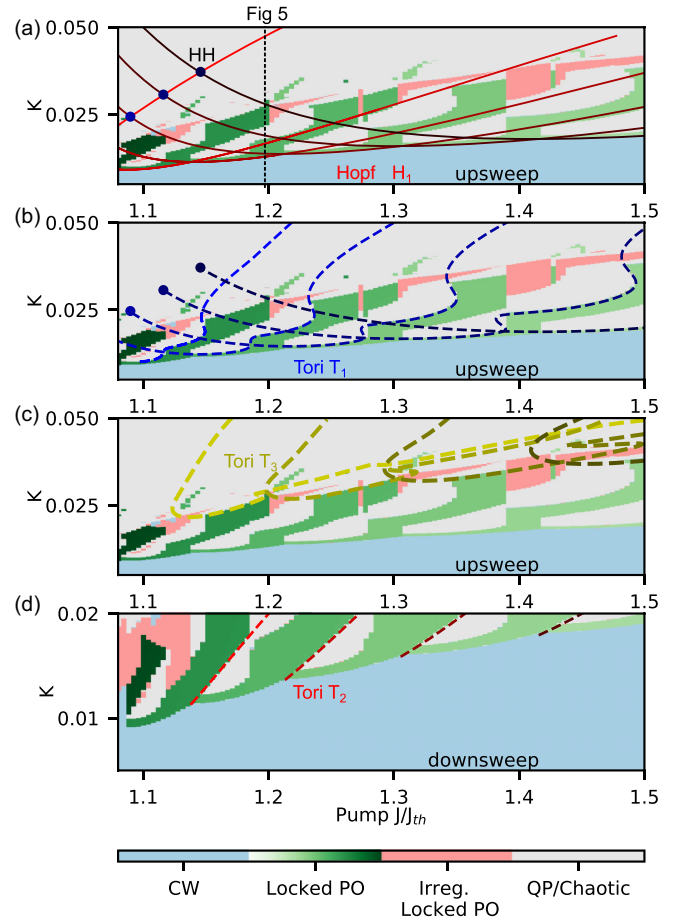


FIG. 7. Two-dimensional bifurcation diagrams in the (J, K) parameter plane, with the different dynamics distinguished by the color code. The green shading of the regular periodic solutions (pulsed) refers to the different oscillation frequencies. The red areas describe pulsed dynamics which is slightly irregular, similar to the time series shown in Fig. 3(h). (a)–(c) Upsweep in the feedback strength and (d) downswEEP. The red lines in (a) are the Hopf bifurcation lines corresponding to the first Hopf bifurcation H_1 along the cw branch (see Fig. 5) found at different pump currents. The crossing points (HH, blue circles top left) of these Hopf lines give birth to the torus lines (dashed lines) shown in (b), representing the upper stability boundary T_1 of the first periodic orbit PO_1 , as shown exemplarily for $J/J_{th} = 1.19$ in Fig. 6(b). The dashed lines in (c) and (d) represent the upper and lower stability boundaries of the second periodic solution PO_2 , i.e., the tori T_2 and T_3 in Fig. 6(b). All parameters are as in Table I.

threshold and has the fundamental ECM frequency. The T_1 bifurcations in turn give birth to quasiperiodic solutions (gray areas) in between the regular periodic orbits (green areas between $0.125 < K < 0.038$). At higher feedback strength these quasiperiodic regimes become unstable and a second regular periodic orbit stabilizes. The stability boundary of these periodic orbits is given by two torus bifurcations as indicated by T_2 and T_3 in Fig. 6(b). The bifurcation lines of these torus bifurcations are shown as red and yellow dashed lines in Figs. 7(d) and 7(c), respectively. In order to numerically unravel the lower stability boundary (T_2) a downswEEP was computed in Fig. 7(d). This is necessary as the intermediate

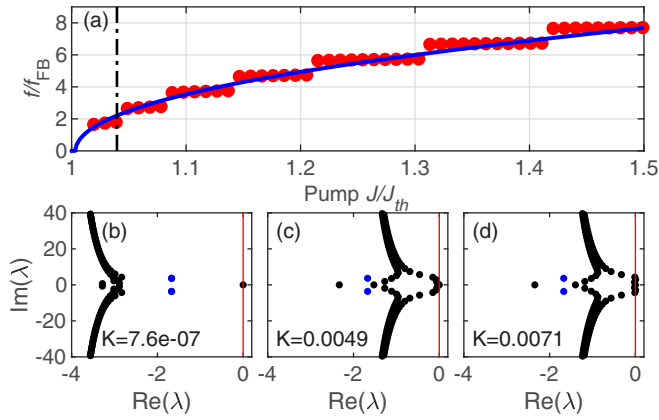


FIG. 8. (a) Relaxation oscillation frequency (blue line) and frequency of the periodic orbit (red circles) generated by the first Hopf bifurcation H_1 along the cw branch (cf. Fig. 6) as a function of the pump current and normalized to the feedback frequency $f_{FB} = 1/\tau$. (b)–(d) Real and imaginary parts of the eigenvalue along the cw solution for increasing feedback strengths, with (d) showing the Hopf point. The eigenvalues corresponding to the relaxation oscillation frequency are marked in blue. The pump current is set to $J/J_{th} = 1.04$, as marked by the vertical black line in (a). All parameters are as in Table I.

quasiperiodic regime emerges directly from the first periodic orbit in T_1 and therefore the system directly stabilizes onto it in the upsweeps shown in Figs. 7(a)–7(c). The difference in the sweeps also unravels the multistability between the quasiperiodic and periodic states.

VI. STAIRCASE PERIOD CHANGES

In the following, we investigate the frequency of the first stable periodic orbit and its relation to the relaxation oscillation frequency. We therefore find the frequency of the periodic orbit at the first Hopf point in K at increasing pump currents and also determine the relaxation oscillation frequency for the respective pump current. The periodic orbit's frequency is indicated by red circles in Fig. 8(a), whereas the dependence of the RO frequency is given by the blue line. We obtain the results by extracting the eigenvalue spectrum of the cw steady state, applying a linear stability analysis using DDE-BIFTOOL. The imaginary part of the nontrivial eigenvalues λ existing at $K = 0$ corresponds to the relaxation oscillation frequency via the relation $f_{RO} = \text{Im}(\lambda)/2\pi$, whereas the imaginary part of the eigenvalue pair crossing the imaginary axis at K_{Hopf} relates to the Hopf frequency. The eigenvalue spectrum is displayed in Figs. 8(b)–8(d) for three feedback strengths at the pump current indicated by the black line in Fig. 8(a). The eigenvalue pair corresponding to the RO frequency is marked in blue.

The RO frequency shows a square root dependence [see Fig. 8(a)] on the pump current, whereas the frequency of the periodic orbit follows a staircase behavior in which the frequency always increases in steps of the feedback or external cavity frequency f_{FB} . Hence, we can deduce that the eigenvalue pair with the frequency closest to the RO leads to the stabilization of the periodic orbit via a Hopf bifurcation. This is also supported by the eigenvalues in Figs. 8(b)–8(d), where the eigenvalue pair with an imaginary part closest to the

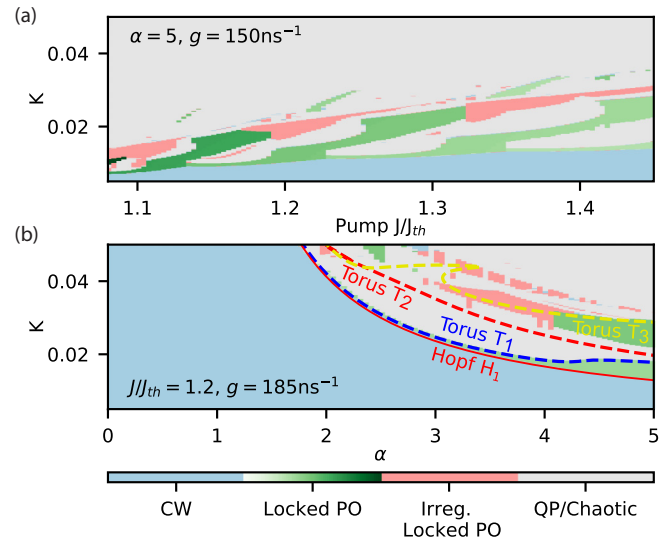


FIG. 9. (a) Two-dimensional bifurcation diagrams in the (J, K) parameter plane, with the different dynamics distinguished by the color code as in Fig. 7, but for a lower gain $g = 150$. (b) Two-dimensional bifurcation diagrams in the (α, K) parameter plane. The solid line marks the bifurcation line of the first Hopf bifurcation H_1 and the dashed lines correspond to the torus bifurcations T_{1-3} as displayed in Fig. 6(b) (1D cut at $\alpha = 5$). The pump current is $J/J_{th} = 1.19$; all other parameters are as in Table I.

ROs (blue circles) crosses the imaginary axis first. Due to the coupling between the bulk reservoir and the SMLQD states, the investigated device inhibits a high damping, which was argued to be a key property necessary for the locked periodic orbits to occur [26]. Hence, the presented explanation of the stepwise frequency change also applies to the staircase scenario found in the measurements obtained using a quantum-dot device in [26]. One can also understand the discussed locking effect in terms of a destabilization of the cw lasing. Above a critical feedback strength the excess depletion of the gain resulting from the feedback intensity cannot be compensated and therefore the cw state destabilizes to a periodic orbit. With increasing pump current the relaxation oscillation frequency shifts to higher values and therefore higher periods are favored, as shown before. As the RO frequency is strongly influenced by the gain factor g , the latter also influences the locking frequency. This is supported by the 2D bifurcation diagram in the (J, K) plane in Fig. 9(a) calculated with a reduced g . Here the areas of single periodic orbits stretch over a higher relative pump current and the transitions to higher oscillation frequencies are shifted to higher pump currents. The reason for that lies within a slower increase of the RO frequency with increasing pump current, due to the reduced gain.

The investigations of laser diodes with quantum-dot, quantum-well, or bulk gain all show that a high α -factor is very beneficial for the locking oscillations to occur [25,26,30,31,39]. We obtain similar findings as the bifurcation diagram in the (α, K) plane [Fig. 9(b)] shows that the periodic orbits are completely lost for feedback levels $K < 0.05$ if the α -factor is reduced below $\alpha < 2$. This results from the Hopf bifurcation H_1 and the torus bifurcation T_1 , enclosing the stable region of periodic locked orbits, strongly

shifting to high feedback strengths with decreasing α -factor. Furthermore, these bifurcations approach each other as α is scaled down and hence reduce the region of stable periodic orbits. At this point we highlight that a high α is required by the theoretical model to correctly model the properties of the SMLQD gain system. Additionally, we note that the second regime of regular periodic pulslike dynamics turns to an irregular behavior at decreasing α values, as indicated in Fig. 9(b). Similar results were also acquired for the stability boundaries of the ECMs of a bulk laser diode investigated in [39], supporting that the feedback has a more dominant effect on the locking as compared to the gain material.

VII. CONCLUSION

We have presented an experimental and theoretical investigation of a semiconductor laser with strong amplitude-phase coupling subject to optical feedback at an intermediate feedback length of $\tau = 3.8$ ns, using submonolayer quantum dots as the active medium. We presented a theoretical model for a SMLQD laser diode subject to optical feedback, which correctly describes the damping and relaxation oscillations by the coupling of the bulk reservoir and SMLQD states. To ensure the usage of realistic SMLQD laser parameters, we started from the values found on similar samples in our previous works [52,55] and only slightly altered these values in the course of correctly reproducing the relaxation oscillations of the experimentally investigated device. Utilizing this model, we were able to reproduce an experimentally obtained phase-locking effect at intermediate feedback strengths, which leads to a periodic pulslike laser output. This also allowed us to complement our experimental findings by a theory exploring the stepwise frequency change of the periodic orbits with increasing pump current. Specifically, our results showed that the step size is always related to the inverse feedback time and is induced by the eigenvalue pair closest to the relaxation oscillation frequency stabilizing the respective periodic orbit. This can be generalized to previous experiments on quantum-dot and quantum-well lasers [25,26], as the high damping of the devices seems to be the most important requirement for the locking effect, which is predominantly induced by the feedback. A comparison of our findings to the existing literature also suggested that a high α -factor and intermediate feedback lengths $1 \text{ ns} < \tau < 10 \text{ ns}$ close to the relaxation oscillation frequency seem to be beneficial for these type of oscillations to occur. Furthermore, we performed an in-depth bifurcation analysis showing that torus bifurcations lead to a stabilization of further periodic branches at higher feedback strengths and the intermediate transition to a quasiperiodic laser output. The generalization of the underlying feedback effect with a stepwise change in period can be of interest for the future development of tunable photonic microwave sources that only rely on a simple form of energy efficient feedback [34,61,62]. Additionally, our findings give further insight into the optimal operation points of SMLQD lasers, if optical feedback cannot be prevented and comes as a destabilizing effect.

ACKNOWLEDGMENTS

The authors thank the Deutsche Forschungsgemeinschaft within the frame of the Sonderforschungsbereich787 (all) and Sonderforschungsbereich910 (J.H. and K.L.) for funding.

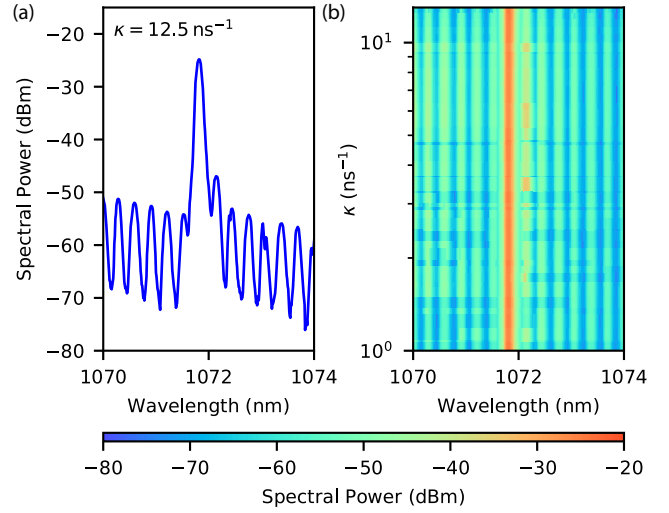


FIG. 10. (a) Experimentally obtained optical spectrum of the SMLQD device at a feedback rate of $\kappa = 12.5 \text{ ns}^{-1}$. (b) Optical spectra of the SMLQD device at different feedback rates; the spectral power is given by the color code.

APPENDIX A: MODELING THE EQUILIBRIUM DISTRIBUTION

The SMLQD equilibrium occupation probability $\rho_{\text{eq}}(t, n)$ is determined by a quasi-Fermi distribution

$$\rho_{\text{eq}}(t, n) = \left[\exp\left(\frac{\bar{\epsilon}_{\text{SML}} - E_{\text{F}}(t, n)}{k_{\text{B}}T}\right) + 1 \right]^{-1}, \quad (\text{A1})$$

where $\bar{\epsilon}_{\text{SML}}$ is the mean SMLQD confinement energy with respect to the bulk reservoir band edge, m^* is the effective mass, T is the lattice temperature, and E_{F} is the quasiequilibrium Fermi level, which is determined via the Padé approximation [77]:

$$E_{\text{F}}(t, n) = k_{\text{B}}T (\ln[\tilde{n}(t)] + A_1 \tilde{n}(t) + \{K_1 \ln[1 + K_2 \tilde{n}(t)] - K_1 K_2 \tilde{n}(t)\}), \quad (\text{A2})$$

with $\tilde{n}(t) = n(t)/n_{\text{C}}$, where the effective density of states n_{C} is given by

$$n_{\text{C}} = 2 \left(\frac{m^* k_{\text{B}}T}{2\pi \hbar^2} \right)^{3/2}. \quad (\text{A3})$$

The coefficients are $A_1 = 1/\sqrt{8}$, $A_2 = -4.95009 \times 10^{-3}$, $K_1 = 4.7$, and $K_2 = \sqrt{2|A_2|/K_1}$, taken from [77].

APPENDIX B: MAXIMUM FEEDBACK RATE

In order to give a measure of the effective feedback rate κ , we calculate the maximum effective feedback rate κ_{max} for the investigated etalon mode as

$$\kappa_{\text{max}} = \frac{1 - R_{\text{GaAs}}}{\tau_{\text{LD}}} \frac{E_{\text{ph}}}{e_0} \left[\left(\frac{\delta I}{\delta P} \right)_{\text{EC}} - \left(\frac{\delta I}{\delta P} \right)_{\text{LD}} \right], \quad (\text{B1})$$

where $R_{\text{GaAs}} = 0.33$ is the reflectivity of the GaAs facet, $E_{\text{ph}} = 1.16 \text{ eV}$ is the photon energy, $\tau_{\text{LD}} = 12 \text{ ps}$ is the round-trip time of the laser diode, e_0 is the electron charge, and $(\frac{\delta I}{\delta P})_{\text{LD,EC}}$ refers to the fitted linear slope of the P - I laser curve of the free-running laser diode (LD) and the laser under maximum feedback (EC). By utilizing the attenuation resulting

from the double pass of the neutral density filter β (in dB), we determine the effective feedback rate as follows:

$$\kappa = \kappa_{\max} 10^{\beta/10}. \quad (\text{B2})$$

APPENDIX C: MODE SELECTION

Including an etalon in the feedback cavity allows us to select single laser modes for the optical feedback as indicated

in Fig. 1(b). This induces a stable single-mode operation of the SMLQD laser device at the chosen mode, starting at low feedback rates. This is indicated in Fig. 10: Fig. 10(a) shows an experimentally determined spectrum at a feedback rate of $\kappa = 12.5 \text{ ns}^{-1}$ and Fig. 10(b) displays the evolution of the optical spectrum while changing the feedback rate. In both images a side-mode compression is clearly visible when comparing the spectrum to the one of the free-running laser in Fig. 1(b).

-
- [1] M. Grundmann, *Nano-Optoelectronics: Concepts, Physics and Devices* (Springer, Berlin, 2002).
- [2] J. Ohtsubo, *Semiconductor Lasers: Stability, Instability and Chaos*, 3rd ed. (Springer, Berlin, 2013).
- [3] R. Tkach and A. Chraplyvy, Regimes of feedback effects in 1.5- μm distributed feedback lasers, *J. Lightwave Technol.* **4**, 1655 (1986).
- [4] B. Dahmani, L. Hollberg, and R. Drullinger, Frequency stabilization of semiconductor lasers by resonant optical feedback, *Opt. Lett.* **12**, 876 (1987).
- [5] A. Ahlborn and U. Parlitz, Chaos Control using Notch Feedback, *Phys. Rev. Lett.* **96**, 034102 (2006).
- [6] T. Dahms, P. Hövel, and E. Schöll, Stabilizing continuous-wave output in semiconductor lasers by time-delayed feedback, *Phys. Rev. E* **78**, 056213 (2008).
- [7] C.-F. Chuang, Y.-H. Liao, C.-H. Lin, S.-Y. Chen, F. Grillot, and F.-Y. Lin, Linewidth enhancement factor in semiconductor lasers subject to various external optical feedback conditions, *Opt. Express* **22**, 5651 (2014).
- [8] D. Brunner, R. Luna, A. Delhom i Latorre, X. Porte, and I. Fischer, Semiconductor laser linewidth reduction by six orders of magnitude via delayed optical feedback, *Opt. Lett.* **42**, 163 (2017).
- [9] G. P. Agrawal, Line narrowing in a single-mode injection-laser due to external optical feedback, *IEEE J. Quantum Electron.* **20**, 468 (1984).
- [10] D. Arsenijević, M. Kleinert, and D. Bimberg, Phase noise and jitter reduction by optical feedback on passively mode-locked quantum-dot lasers, *Appl. Phys. Lett.* **103**, 231101 (2013).
- [11] C. Otto, K. Lüdge, A. G. Vladimirov, M. Wolfrum, and E. Schöll, Delay induced dynamics and jitter reduction of passively mode-locked semiconductor laser subject to optical feedback, *New J. Phys.* **14**, 113033 (2012).
- [12] L. C. Jaurigue, E. Schöll, and K. Lüdge, Suppression of Noise-Induced Modulations in Multidelay Systems, *Phys. Rev. Lett.* **117**, 154101 (2016).
- [13] C. Y. Lin, F. Grillot, and Y. Li, Microwave characterization and stabilization of timing jitter in a quantum dot passively mode-locked laser via external optical feedback, *IEEE J. Sel. Top. Quantum Electron.* **17**, 1311 (2011).
- [14] Y. Cho and T. Umeda, Chaos in laser oscillations with delayed feedback: Numerical analysis and observation using semiconductor lasers, in *International Quantum Electronics Conference*, edited by H. Koglnik, Y. Shen, M. Richardson, and C. Tang, OSA Technical Digest (Optical Society of America, 1984), paper WEE2.
- [15] F. Albert, C. Hopfmann, S. Reitzenstein, C. Schneider, S. Höfling, L. Worschech, M. Kamp, W. Kinzel, A. Forchel, and I. Kanter, Observing chaos for quantum-dot microlasers with external feedback, *Nat. Commun.* **2**, 366 (2011).
- [16] K. Al-Naimee, F. Marino, M. Ciszak, R. Meucci, and F. T. Arecchi, Chaotic spiking and incomplete homoclinic scenarios in semiconductor lasers with optoelectronic feedback, *New J. Phys.* **11**, 073022 (2009).
- [17] J. Ohtsubo, Feedback induced instability and chaos in semiconductor lasers and their applications, *J. Opt. Rev.* **6**, 1 (1999).
- [18] G. Bouchez, C. H. Uy, B. Macias, D. Wolfersberger, and M. Sciamanna, Wideband chaos from a laser diode with phase-conjugate feedback, *Opt. Lett.* **44**, 975 (2019).
- [19] C. R. Mirasso, P. Colet, and P. Garcia-Fernandez, Synchronization of chaotic semiconductor lasers: Application to encoded communications, *IEEE Photon. Technol. Lett.* **8**, 299 (1996).
- [20] T. Heil, J. Mulet, I. Fischer, C. R. Mirasso, M. Peil, P. Colet, and W. Elsässer, On/off phase shift keying for chaos-encrypted communication using external-cavity semiconductor lasers, *IEEE J. Quantum Electron.* **38**, 1162 (2002).
- [21] L. Appeltant, M. C. Soriano, G. Van der Sande, J. Danckaert, S. Massar, J. Dambre, B. Schrauwen, C. R. Mirasso, and I. Fischer, Information processing using a single dynamical node as complex system, *Nat. Commun.* **2**, 468 (2011).
- [22] J. Bueno, D. Brunner, M. C. Soriano, and I. Fischer, Conditions for reservoir computing performance using semiconductor lasers with delayed optical feedback, *Opt. Express* **25**, 2401 (2017).
- [23] L. Larger, A. Baylón-Fuentes, R. Martinenghi, V. S. Udaltsov, Y. K. Chembo, and M. Jacquot, High-Speed Photonic Reservoir Computing Using a Time-Delay-Based Architecture: Million Words per Second Classification, *Phys. Rev. X* **7**, 011015 (2017).
- [24] F. Köster, D. Ehlert, and K. Lüdge, Limitations of the recall capabilities in delay-based reservoir computing systems, *Cogn Comput* (2020), doi: 10.1007/s12559-020-09733-5.
- [25] B. Tykalewicz, D. Goulding, S. P. Hegarty, G. Huyet, T. Erneux, B. Kelleher, and E. A. Viktorov, Emergence of resonant mode-locking via delayed feedback in quantum dot semiconductor lasers, *Opt. Express* **24**, 4239 (2016).
- [26] B. Kelleher, M. J. Wishon, A. Locquet, D. Goulding, B. Tykalewicz, G. Huyet, and E. A. Viktorov, Delay induced high order locking effects in semiconductor lasers, *Chaos* **27**, 114325 (2017).

- [27] J. Mørk, B. Tromborg, and J. Mark, Chaos in semiconductor lasers with optical feedback—Theory and experiment, *IEEE J. Quantum Electron.* **28**, 93 (1992).
- [28] J. Helms and K. Petermann, A simple analytic expression for the stable operation range of laser diodes with optical feedback, *IEEE J. Quantum Electron.* **26**, 833 (1990).
- [29] A. Ritter and H. Haug, Theory of laser diodes with weak optical feedback. II. Limit-cycle behavior, quasi-periodicity, frequency locking, and route to chaos, *J. Opt. Soc. Am. B* **10**, 145 (1993).
- [30] D. Pieroux, T. Erneux, B. Haegeman, K. Engelborghs, and D. Roose, Bridges of Periodic Solutions and Tori in Semiconductor Lasers Subject to Delay, *Phys. Rev. Lett.* **87**, 193901 (2001).
- [31] H. Erzgräber, B. Krauskopf, D. Lenstra, A. P. A. Fischer, and G. Vemuri, Frequency versus relaxation oscillations in a semiconductor laser with coherent filtered optical feedback, *Phys. Rev. E* **73**, 055201 (2006).
- [32] B. Kim, A. Locquet, D. Choi, and D. S. Citrin, Experimental route to chaos of an external-cavity semiconductor laser, *Phys. Rev. A* **91**, 061802(R) (2015).
- [33] A. V. Kovalev, M. S. Islam, A. Locquet, D. S. Citrin, E. A. Viktorov, and T. Erneux, Resonances between fundamental frequencies for lasers with large delayed feedbacks, *Phys. Rev. E* **99**, 062219 (2019).
- [34] M. S. Islam, A. V. Kovalev, G. Coget, E. A. Viktorov, D. S. Citrin, and A. Locquet, Staircase Dynamics of a Photonic Microwave Oscillator Based on a Laser Diode with Delayed Optoelectronic Feedback, *Phys. Rev. Appl.* **13**, 064038 (2020).
- [35] A. A. Tager and K. Petermann, High-frequency oscillations and self-mode locking in short external-cavity laser diodes, *IEEE J. Quantum Electron.* **30**, 1553 (1994).
- [36] A. P. A. Fischer, M. Yousefi, D. Lenstra, M. W. Carter, and G. Vemuri, Filtered Optical Feedback Induced Frequency Dynamics in Semiconductor Lasers, *Phys. Rev. Lett.* **92**, 023901 (2004).
- [37] A. Hohl, H. J. C. van der Linden, and R. Roy, Determinism and stochasticity of power-dropout events in semiconductor lasers with optical feedback, *Opt. Lett.* **20**, 2396 (1995).
- [38] T. Heil, I. Fischer, and W. Elsässer, Coexistence of low-frequency fluctuations and stable emission on a single high-gain mode in semiconductor lasers with external optical feedback, *Phys. Rev. A* **58**, R2672 (1998).
- [39] B. Haegeman, K. Engelborghs, D. Roose, D. Pieroux, and T. Erneux, Stability and rupture of bifurcation bridges in semiconductor lasers subject to optical feedback, *Phys. Rev. E* **66**, 046216 (2002).
- [40] D. Waldburger, S. M. Link, M. Mangold, C. G. E. Alfieri, E. Gini, M. Golling, B. W. Tilma, and U. Keller, High-power 100 fs semiconductor disk lasers, *Optica* **3**, 844 (2016).
- [41] M. A. Gaafar, A. Rahimi-Iman, K. A. Fedorova, W. Stolz, E. U. Rafailov, and M. Koch, Mode-locked semiconductor disk lasers, *Adv. Opt. Photon.* **8**, 370 (2016).
- [42] C. Ma, C. Wang, B. Gao, J. Adams, G. Wu, and H. Zhang, Recent progress in ultrafast lasers based on 2D materials as a saturable absorber, *Appl. Phys. Rev.* **6**, 041304 (2019).
- [43] T. Herr, V. Brasch, J. D. Jost, C. Wang, N. Kondratiev, M. Gorodetsky, and T. Kippenberg, Temporal solitons in optical microresonators, *Nat. Photon.* **8**, 145 (2014).
- [44] Y. Song, X. Shi, C. Wu, D. Tang, and H. Zhang, Recent progress of study on optical solitons in fiber lasers, *Appl. Phys. Rev.* **6**, 021313 (2019).
- [45] Y. Song, Z. Wang, C. Wang, K. Panajotov, and H. Zhang, Recent progress on optical rogue waves in fiber lasers: Status, challenges, and perspectives, *Adv. Photon.* **2**, 024001 (2020).
- [46] A. F. Tsatsulnikov, B. V. Volovik, N. N. Ledentsov, M. V. Maximov, A. Y. Egorov, A. R. Kovsh, V. M. Ustinov, A. E. Zhukov, P. S. Kop'ev, Z. I. Alferov, I. A. Kozin, M. V. Belousov, I. P. Soshnikov, P. Werner, D. Litvinov, U. Fischer, A. Rosenauer, and D. Gerthsen, Lasing in structures with InAs quantum dots in an (Al,Ga)As matrix grown by submonolayer deposition, *J. Electron. Mater.* **28**, 537 (1999).
- [47] I. Krestnikov, M. Straßburg, M. Caesar, A. Hoffmann, U. W. Pohl, D. Bimberg, N. Ledentsov, P. S. Kop'ev, Z. I. Alferov, D. Litvinov, A. Rosenauer, and D. Gerthsen, Control of the electronic properties of CdSe submonolayer superlattices via vertical correlation of quantum dots, *Phys. Rev. B* **60**, 8695 (1999).
- [48] W. W. Chow and F. Jahnke, On the physics of semiconductor quantum dots for applications in lasers and quantum optics, *Prog. Quantum Electron.* **37**, 109 (2013).
- [49] F. Jahnke, *Quantum Optics with Semiconductor Nanostructures* (Woodhead, Cambridge, 2012).
- [50] N. Owschmikow, B. Herzog, B. Lingnau, K. Lüdge, A. Lenz, H. Eisele, M. Dähne, T. Niermann, M. Lehmann, A. Schliwa, A. Strittmatter, and U. W. Pohl, in *Semiconductor Nanophotonics: Materials, Models, and Devices*, edited by M. Kneissl, A. Knorr, S. Reitzenstein, and A. Hoffmann, Springer Series in Solid-State Sciences Vol. 194 (Springer International, Cham, 2020), Chap. 2, pp. 13–51.
- [51] D. Arsenijević, C. Y. Liu, A. Payusov, M. Stubenrauch, and D. Bimberg, Temperature-dependent characteristics of single-mode InAs submonolayer quantum-dot lasers, *IEEE Photon. Technol. Lett.* **24**, 906 (2012).
- [52] B. Lingnau, K. Lüdge, B. Herzog, M. Kolarczik, Y. Kaptan, U. Woggon, and N. Owschmikow, Ultrafast gain recovery and large nonlinear optical response in submonolayer quantum dots, *Phys. Rev. B* **94**, 014305 (2016).
- [53] B. Herzog, N. Owschmikow, J. H. Schulze, R. Rosales, Y. Kaptan, M. Kolarczik, T. Switański, A. Strittmatter, D. Bimberg, U. W. Pohl, and U. Woggon, Fast gain and phase recovery of semiconductor optical amplifiers based on submonolayer quantum dots, *Appl. Phys. Lett.* **107**, 201102 (2015).
- [54] S. Harrison, M. P. Young, P. D. Hodgson, R. J. Young, M. Hayne, L. Danos, A. Schliwa, A. Strittmatter, A. Lenz, U. W. Pohl, and D. Bimberg, Heterodimensional charge-carrier confinement in stacked submonolayer InAs in GaAs, *Phys. Rev. B* **93**, 085302 (2016).
- [55] B. Herzog, B. Lingnau, M. Kolarczik, Y. Kaptan, D. Bimberg, A. Maaßdorf, U. W. Pohl, R. Rosales, J. H. Schulze, A. Strittmatter, M. Weyers, U. Woggon, K. Lüdge, and N. Owschmikow, Strong amplitude-phase coupling in submonolayer quantum dots, *Appl. Phys. Lett.* **109**, 201102 (2016).
- [56] B. Herzog, B. Lingnau, M. Kolarczik, S. Helmrich, A. Achtstein, K. Thommes, F. Alhusein, D. Quandt, A. Strittmatter, U. W. Pohl, O. Brox, M. Weyers, U. Woggon, K. Lüdge, and N. Owschmikow, Broadband semiconductor light sources operating at 1060 nm based on InAs:Sb/GaAs submonolayer quantum dots, *IEEE J. Sel. Top. Quantum Electron.* **25**, 1900310 (2019).
- [57] I. L. Krestnikov, N. N. Ledentsov, A. Hoffmann, and D. Bimberg, Arrays of two-dimensional islands formed by sub-

- monolayer insertions: Growth, properties, devices, *Phys. Status Solidi A* **183**, 207 (2001).
- [58] Z. Xu, D. Birkedal, M. Juhl, and J. M. Hvam, Submonolayer InGaAs/GaAs quantum-dot lasers with high modal gain and zero-linewidth enhancement factor, *Appl. Phys. Lett.* **85**, 3259 (2004).
- [59] V. V. Dudelev, N. A. Maleev, A. G. Kuz'menkov, S. A. Blokhin, V. Y. Myl'nikov, V. I. Kuchinskii, V. M. Ustinov, E. U. Rafailov, and G. S. Sokolovskii, Peaking of optical pulses in vertical-cavity surface-emitting lasers with an active region based on submonolayer InGaAs quantum dots, *Tech. Phys. Lett.* **43**, 1099 (2017).
- [60] C. G. E. Alfieri, D. Waldburger, R. Nürnberg, M. Golling, L. C. Jaurigue, K. Lüdge, and U. Keller, Mode-Locking Instabilities for High-Gain Semiconductor Disk Lasers Based on Active Submonolayer Quantum Dots, *Phys. Rev. Appl.* **10**, 044015 (2018).
- [61] M. J. Chacron, B. Lindner, and A. Longtin, Noise Shaping by Interval Correlations Increases Information Transfer, *Phys. Rev. Lett.* **92**, 080601 (2004).
- [62] P. Pérez, A. Quirce, A. Valle, A. Consoli, I. Noriega, L. Pesquera, and I. Esquivias, Photonic generation of microwave signals using a single-mode VCSEL subject to dual-beam orthogonal optical injection, *IEEE Photon. J.* **7**, 5500614 (2015).
- [63] A. Wilms, D. Breddermann, and P. Mathe, Theory of direct capture from two- and three-dimensional reservoirs to quantum dot states, *Phys. Status Solidi C* **9**, 1278 (2012).
- [64] R. Lang and K. Kobayashi, External optical feedback effects on semiconductor injection laser properties, *IEEE J. Quantum Electron.* **16**, 347 (1980).
- [65] S. Yanchuk and M. Wolfrum, A multiple time scale approach to the stability of external cavity modes in the Lang-Kobayashi system using the limit of large delay, *SIAM J. Appl. Dyn. Syst.* **9**, 519 (2010).
- [66] V. Rottschäfer and B. Krauskopf, The ECM-backbone of the Lang-Kobayashi equations: A geometric picture, *Int. J. Bifurcat. Chaos* **17**, 1575 (2007).
- [67] G. Ortner, C. N. Allen, C. Dion, P. Barrios, D. Poitras, D. Dalacu, G. Pakulski, J. Lapointe, P. J. Poole, and W. Render, External cavity InAs/InP quantum dot laser with a tuning range of 166 nm, *Appl. Phys. Lett.* **88**, 121119 (2006).
- [68] T. Erneux, G. H. M. van Tartwijk, D. Lenstra, and A. M. Levine, Determining Lang and Kobayashi Hopf bifurcation points, in *Proceeding of SPIE*, Physics and Simulation of Optoelectronic Devices III, Vol. 2399 (SPIE, 1995).
- [69] P. M. Alsing, V. Kovanis, A. Gavrielides, and T. Erneux, Lang and Kobayashi phase equation, *Phys. Rev. A* **53**, 4429 (1996).
- [70] L. D. Westbrook, N. C. Fletcher, D. M. Cooper, M. Stevenson, and P. C. Spurdens, Intensity noise in 1.5 μm GaInAs quantum well buried heterostructure lasers, *Electron. Lett.* **25**, 1183 (1989).
- [71] B. Lingnau, K. Lüdge, W. W. Chow, and E. Schöll, Influencing modulation properties of quantum-dot semiconductor lasers by electron lifetime engineering, *Appl. Phys. Lett.* **101**, 131107 (2012).
- [72] K. Engelborghs, T. Luzyanina, and D. Roose, Numerical bifurcation analysis of delay differential equations using DDE-BIFTOOL, *ACM Trans. Math. Softw.* **28**, 1 (2002).
- [73] S. G. Abdulrhmann, M. Ahmed, T. Okamoto, W. Ishimori, and M. Yamada, An improved analysis of semiconductor laser dynamics under strong optical feedback, *IEEE J. Sel. Top. Quantum Electron.* **9**, 1265 (2003).
- [74] A. Tabaka, K. Panajotov, I. Veretennicoff, and M. Sciamanna, Bifurcation study of regular pulse packages in laser diodes subject to optical feedback, *Phys. Rev. E* **70**, 036211 (2004).
- [75] J. Mørk, J. Mark, and B. Tromborg, Route to Chaos and Competition between Relaxation Oscillations for a Semiconductor Laser with Optical Feedback, *Phys. Rev. Lett.* **65**, 1999 (1990).
- [76] G. Lythe, T. Erneux, A. Gavrielides, and V. Kovanis, Low pump limit of the bifurcation to periodic intensities in a semiconductor laser subject to external optical feedback, *Phys. Rev. A* **55**, 4443 (1997).
- [77] L. A. Coldren and S. W. Corzine, *Diode Lasers and Photonic Integrated Circuits* (Wiley, New York, 1995).